Published in final edited form as:
Sci Transl Med. 2012 May 2; 4(132): . doi:10.1126/scitranslmed.3003787.

Vascular COX-2 Modulates Blood Pressure and Thrombosis in Mice

Ying Yu[1,*,†,‡], **Emanuela Ricciotti**[1,*], **Rosario Scalia**[2], **Soon Yew Tang**[1], **Gregory Grant**[1], **Zhou Yu**[1], **Gavin Landesberg**[2], **Irene Crichton**[3], **Weichen Wu**[1], **Ellen Puré**[3], **Colin D. Funk**[4], and **Garret A. FitzGerald**[1,‡]

[1]Institute for Translational Medicine and Therapeutics, University of Pennsylvania, Philadelphia, PA 19104, USA.

[2]Department of Physiology, Temple University, Philadelphia, PA 19140, USA.

[3]Wistar Institute, Philadelphia, PA 19104, USA.

[4]Department of Biomedical and Molecular Sciences, Queen's University, Kingston, Ontario K7L 3N6, Canada.

Abstract

Prostacyclin (PGI_2) is a vasodilator and platelet inhibitor, properties consistent with cardioprotection. More than a decade ago, inhibition of cyclooxygenase-2 (COX-2) by the nonsteroidal anti-inflammatory drugs (NSAIDs) rofecoxib and celecoxib was found to reduce the amount of the major metabolite of PGI_2 (PGI-M) in the urine of healthy volunteers. This suggested that NSAIDs might cause adverse cardiovascular events by reducing production of cardioprotective PGI_2. This prediction was based on the assumption that the concentration of PGI-M in urine likely reflected vascular production of PGI_2 and that other cardioprotective mediators, especially nitric oxide (NO), were not able to compensate for the loss of PGI_2. Subsequently, eight placebo-controlled clinical trials showed that NSAIDs that block COX-2 increase adverse cardiovascular events. We connect tissue-specific effects of NSAID action and functional correlates in mice with clinical outcomes in humans by showing that deletion of COX-2 in the mouse vasculature reduces excretion of PGI-M in urine and predisposes the animals to both hypertension and thrombosis. Furthermore, vascular disruption of COX-2 depressed expression of endothelial NO synthase and the consequent release and function of NO. Thus, suppression of PGI_2 formation resulting from deletion of vascular COX-2 is sufficient to explain the cardiovascular hazard from NSAIDs, which is likely to be augmented by secondary mechanisms such as suppression of NO production.

INTRODUCTION

During the development of nonsteroidal anti-inflammatory drugs (NSAIDs) selective for inhibition of cyclooxygenase-2 (COX-2), we found that they suppressed biosynthesis of the

‡To whom correspondence should be addressed. garret@upenn.edu (G.A.F.); yuying@sibs.ac.cn (Y.Y.).
*These authors contributed equally to this work.
†Present address: Key Laboratory of Nutrition and Metabolism, Institute for Nutritional Sciences, Shanghai Institutes for Biological Sciences, Chinese Academy of Sciences, Shanghai 200031, China.

Author contributions: Y.Y., E.R., and G.A.F. conceived and designed the experiments and coordinated the work presented. Y.Y., E.R., R.S., S.Y.T., G.L., I.C., Z.Y., and E.P. performed the experiments. G.G. and W.W. analyzed the data. E.P. and C.D.F. commented on and edited the manuscript. Y.Y., E.R., and G.A.F. wrote the manuscript.

Competing interests: G.A.F. has served as a consultant to Lilly and Boehringer Ingelheim in the past year. The other authors declare that they have no competing interests.

prostaglandin I_2 (PGI_2), a potent vasodilator and inhibitor of platelet activation. This was reflected by a decrease in the urinary excretion of its major metabolite, 2,3-dinor-6 keto $PGF_{1\alpha}$ (PGI-M), in healthy volunteers (1, 2). Given the restraint exerted on platelet aggregation and vasoconstriction by PGI_2 in vitro (3), we suggested that this might predispose patients taking these drugs to a cardiovascular hazard. Because COX-2 can be induced by laminar shear in vitro (4), we proposed that the enzyme was up-regulated by blood flow under physiological conditions in vivo, explaining our observations. Although the vascular endothelium has a marked capacity to generate PGI_2 in vitro (3), it has been claimed that urinary PGI-M did not reflect biosynthesis in the vascular compartment (5) and that COX-2 was undetectable in endothelial cells (ECs) in vitro (6). Indeed, it was argued that other mechanisms, chief among them the ability to generate nitric oxide (NO), would compensate for any deficiency of PGI_2. Subsequently, placebo-controlled trials revealed that three structurally distinct NSAIDs selective for inhibition of COX-2—rofecoxib, celecoxib, and valdecoxib—predisposed patients to myocardial infarction and stroke (7). Besides the increase in clinical events, there was an increase in hypertension and heart failure in the treated groups. Despite this and the recapitulation of elements of this hazard in mice lacking the PGI_2 receptor (7, 8), attribution of cause to suppression of COX-2–derived PGI_2 has continued to be debated. It has been suggested that hypertension, due to some ill-defined but independent mechanism, accounted for the impact of NSAIDs on cardiovascular outcomes (7, 9). The detection in observational studies of a cardiovascular hazard from some of the older NSAIDs, such as diclofenac (10, 11), was also used to argue against the mechanistic relevance of selectivity for inhibition of COX-2 (12).

Here, we aim to “close the loop” by showing that deletion of COX-2 in either ECs or vascular smooth muscle cells (VSMCs) in mice suppresses urine excretion of PGI-M but not of other major prostaglandin metabolites and that this predisposes to both thrombosis and hypertension. Furthermore, although suppression of COX-2–derived PGI_2 is the dominant mechanism by which this occurs, we show that COX-2 deletion in the vasculature also results in suppression of endothelial NO synthase (eNOS), disrupting release of NO and acetylcholine-dependent vascular relaxation.

RESULTS

Vascular-specific deletion of COX-2 impairs PGI_2 biosynthesis

Using a Flox-Cre strategy, we generated VSMC- and EC-specific COX-2 knockout mice by crossing COX-$2^{flox/flox}$ (COX-$2^{F/F}$) mice with SM22-Cre and Tie2-Cre transgenic mice, respectively. The Cre-mediated excision of the COX-2 allele and the original COX-2^{flox} allele was confirmed by specific polymerase chain reaction (PCR)–based genotyping assays of tail biopsies (Fig. 1A). Genomic analysis of lung, kidney, and liver supported Cre-mediated recombination of the COX-2^{flox} gene. VSMCs derived from aorta and ECs from lung tissue were cultured and stimulated by lipopolysaccharide (LPS) (Fig. 1, B and C). Although constitutively expressed and induced upon LPS treatment, COX-2 protein was disrupted in both VSMCs and ECs through specific SM22-Cre (VSMCCOX-$2^{-/-}$) and Tie2-Cre (ECCOX-$2^{-/-}$) recombinase, respectively.

The products of vascular COX-2, PGE_2 and PGI_2, were suppressed in VSMCs and in ECs from mice with COX-2 deleted from the vasculature both under basal conditions and after LPS stimulation (fig.S1,A and B). Both COX-1 and COX-2 contribute to PGE_2 formation in vivo, as measured by its stable metabolite, 9,15-dioxo-11α-hydroxy-2,3,4,5-tetranor-prostane-1,20-dioic acid (PGE-M) (13). Excretion of PGI-M in urine was significantly depressed by either VSMC COX-2 deletion (2.2 ± 0.18 ng/mg creatinine versus 3.1 ± 0.29 ng/mg creatinine, $P < 0.05$) or EC COX-2 deletion (2.3 ± 0.11 ng/mg creatinine, $P < 0.05$; Fig. 2A) and was further decreased in EC/VSMC double-knockout mice (1.8 ± 0.15 ng/mg

creatinine, $P < 0.01$; Fig. 2A). This was comparable to the degree of inhibition (~50%) observed after global deletion of COX-2 in mice (gCOX-2 knockout mice). A small but significant decrease in urinary PGE-M was observed in male EC/VSMC double-knockout mice (fig. S2A), whereas urinary thromboxane or PGD_2 metabolites were unaltered in these mutant animals (fig. S2, C and D). Thus, vascular COX-2 is a major contributor to systemic PGI_2 formation under physiological conditions in vivo.

Vascular COX-2 regulates systolic blood pressure homeostasis

Although the trend toward elevation of basal blood pressure failed to attain significance after deletion of COX-2 in vascular cells (EC COX-$2^{-/-}$, 114.0 ± 2.0mmHg;VSMC COX-$2^{-/-}$, 116.0 ± 1.9 mmHg, versus COX-$2^{F/F}$ littermates, 112.0 ± 1.6 mmHg; Fig. 2B), the increase in systolic blood pressure in EC/VSMC double-knockout mice attained significance (119.0 ± 2.0 mmHg; $P < 0.05$; Fig. 2B). This hypertensive phenotype was further augmented when mice were placed on a high-salt diet [ECCOX-$2^{-/-}$, 122.0 ± 1.9 mmHg; VSMC COX-$2^{-/-}$, 123.0 ± 1.6mmHg ($P = 0.05$), versus COX-$2^{F/F}$ littermates, 117.0 ± 2.3 mmHg; EC/VSMC double-knockout mice, 126.0 ± 2.6 mmHg ($P < 0.01$), versus COX-$2^{F/F}$ littermates]. A similar hypertensive phenotype was observed in mice with inducible global COX-2 deletion (iCOX-2 knockout mice) (14) on a high-salt diet compared to their COX-$2^{F/F}$ control littermates (iCOX-2 knockout mice, 121.7 ± 10.3 mmHg, versus COX-$2^{F/F}$, 108.7 ± 16.0 mmHg; $P < 0.05$, using a one-tailed Student's *t* test; fig. S3). This phenotype was not attributable to any specific morphological defects in the vasculature (fig. S4).

A negative correlation was observed between urinary PGI-M (but not other prostanoid metabolites) and blood pressure across all the vascular mutant mice ($r = -0.48$; $P < 0.01$), consistent with the hypothesis that the hypertensive phenotype is a consequence of disruption of COX-2–dependent formation of PGI_2. Indeed, administration of a PGI_2 analog, cicaprost, restored the blood pressure phenotype in the hypertensive iCOX-2 knockout mice to that seen in COX-$2^{F/F}$ controls in which cicaprost at this dose had no effect [iCOX-2 knockout mice + cicaprost, 97.2 ± 20.4mmHg, versus COX-$2^{F/F}$+cicaprost, 100.5±18.5 mmHg; P = not significant (n.s.), using a one-tailed Student's *t* test; fig. S3].

Vascular COX-2 restrains thrombogenesis

The time to vascular occlusion after photochemical injury of the carotid artery was significantly shortened in EC COX-2 knockout mice (56.1 ± 6.5 min), VSMC COX-2 knockout mice (53.1 ± 8.0 min), and EC/VSMC double-knockout mice (45.2 ± 8.7 min) when compared to COX-$2^{F/F}$ control animals (80.1 ± 7.7 min, $P < 0.05$; Fig. 2C).

Suppression of PGI-M (15) by COX-2 knockdown [area under the curve (AUC), $6.5 \times 10^4 \pm 2.0 \times 10^4$ arbitrary units (AU), versus controls, $4.1 \times 10^4 \pm 1.4 \times 10^4$ AU; $P < 0.05$; Fig. 3A] or deletion of the PGI_2 receptor markedly delayed the phase of platelet disaggregation (PGI_2 receptor knockout mice, $10 \times 10^4 \pm 2.5 \times 10^4$ AU, versus controls, $4.2 \times 10^4 \pm 1.2 \times 10^4$ AU; $P < 0.001$; Fig. 3B). The early phase of platelet activation, as reflected by maximal thrombus size or the time to maximal thrombus formation, was not significantly altered in these mutants.

By contrast, maximal thrombus formation was reduced in COX-1 knockdown mice (COX-1 knockdown, $1.06 \times 10^5 \pm 0.09 \times 10^5$ pixels, versus control, $3.26 \times 10^5 \pm 0.8 \times 10^5$ pixels; $P < 0.01$) that mimic the asymmetric impact on thromboxane formation observed with low-dose aspirin in humans (16). Similarly, although the time to maximal thrombus size was unaltered (54.4 ± 8.2 s versus 43.1 ± 9.1 s, P = n.s.), the size of the maximal thrombi was reduced in thromboxane receptor knockout mice (thromboxane receptor knockout mice, $1.45 \times 10^5 \pm 0.9 \times 10^5$ pixels, versus controls, $4.02 \times 10^5 \pm 1.1 \times 10^5$ pixels; $P < 0.001$).

Only the later phase of platelet disaggregation was disrupted in the vascular mutants (Fig. 3C), because the AUC was greater in EC COX-$2^{-/-}$ ($11 \times 10^4 \pm 3.7 \times 10^4$ AU, $P < 0.05$), VSMC COX-$2^{-/-}$ ($7.0 \times 10^4 \pm 1.7 \times 10^4$ AU, $P < 0.05$), and EC/VSMC double-knockout mice ($8.4 \times 10^4 \pm 1.2 \times 10^4$ AU, $P < 0.05$) compared to COX-$2^{F/F}$ control mice ($3.9 \times 10^4 \pm 1.0 \times 10^4$ AU).

COX-2 deletion results in NO-dependent vascular dysfunction

Both single vascular cell and EC/VSMC double deletion of COX-2 resulted in decreased expression of eNOS in mouse aorta [VSMC COX-$2^{-/-}$, 55.2 ± 12.8; ECCOX-$2^{-/-}$, 56.5 ± 12.7; EC/VSMC double-knockout mice, 47.3 ± 26.8 mRNA × 10^7/18*S* rRNA (ribosomal RNA), versus COX-$2^{F/F}$ control mice, 89.4 ± 25.4 mRNA × 10^7/18*S* rRNA; $P < 0.05$; Fig. 4A]. A similar trend was observed in the iCOX-2 knockout mice. Cicaprost administration caused a significant increase in eNOS expression in vasculature obtained from iCOX-2 knockout mice on a high-salt diet, but not in littermate controls (iCOX-2 knockout mice, 71.6 ± 15.6, versus iCOX-2 knockout mice + cicaprost, 111.4 ± 33.4 mRNA × 10^7/18*S* rRNA; $P < 0.05$; COX-$2^{F/F}$ control mice, 99.0 ± 23.8, versus COX-$2^{F/F}$ + cicaprost, 91.5.0 ± 17.5 mRNA × 10^7/18*S* rRNA; P = n.s.; fig. S5). Phenylephrine-mediated constriction of aortic rings from mice with global knockout of COX-2, EC/VSMC double-knockout mice, and COX-$2^{F/F}$ controls was similar. However, endothelium-dependent relaxation in response to acetylcholine was significantly impaired in thoracic aortas from gCOX-2 knockout and EC/VSMC double-knockout mice compared with controls [gCOX-2 knockout, 44.3 ± 5.8%; EC/VSMC double-knockout, 50.6 ± 5.1%, versus COX-$2^{F/F}$, 68.8 ± 2.0% relaxation; $P <$ 0.05, one-way analysis of variance (ANOVA); Fig. 4B]. Relaxation induced by sodium nitroprusside (SNP) was unaltered in the mutant animals (Fig. 4C).

Both global and vascular deletion of COX-2 reduced acetylcholine-induced (10^{-5} M) aortic endothelial production of NO compared with controls (gCOX-2 knockout, 0.38 ± 0.16; EC/VSMC double-knockout, 0.42 ± 0.21, versus COX-$2^{F/F}$ controls, 2.04 ± 0.37 nM/mg; $P <$ 0.05, one-way ANOVA; Fig. 4D). N_ω-nitro-L-arginine methyl ester (L-NAME), a specific NO synthase inhibitor, reduced acetylcholine-induced production of NO in aortas from COX-$2^{F/F}$ control animals to a similar degree (Fig. 4D).

DISCUSSION

This study “closes the loop” on the elucidation of a mechanism that is sufficient to explain the cardiovascular hazard attributable to NSAIDs, namely, suppression of cardioprotective COX-2–derived prostaglandins, especially PGI_2.Our results address the outstanding arguments against this mechanism. First, COX-2 is indeed expressed under physiological conditions in ECs in vivo, and its selective deletion in these cells results in suppression of the same PGI_2 metabolite in mice as that shown to be reduced by the NSAIDs rofecoxib and celecoxib in humans. Despite the controversy, human COX-2 was originally cloned from ECs (17), and it has been detected in mouse and human endothelium by some, albeit not all, investigators (18). COX-2 in VSMCs is also a source of PGI_2, and deletion of COX-2 in ECs, VSMCs, or both predisposes mice to thrombosis in vivo. This is true both in large blood vessels and in the microvasculature. The latter preparation allowed us to parse distinct temporal contributions of COX-1–derived thromboxane A_2 and COX-2–derived PGI_2 to the thrombogenic response to vascular injury. Thus, whereas thromboxane A_2 formation appears largely to influence the immediate process of platelet activation, PGI_2 influenced the later resolution of the signal, which is consistent with an impact of PGI_2 on platelet disaggregation in vitro (19).

Second, COX-2 deletion in vascular cells is sufficient to explain the predisposition to hypertension observed in patients taking NSAIDs. Indeed, urinary PGI-M varied inversely

with blood pressure across all of the mutant mice. This is consistent with the predisposition to hypertension in mice with global deletion or inhibition of COX-2 (20), mice in which COX-1 has been placed under the COX-2 promoter (15), and mice deficient in the PGI_2 receptor (8). Deletion of the E prostanoid receptor 2 also predisposes mice to hypertension (21), but suppression of PGE_2 was less pronounced than that of PGI_2, which was detected only in males lacking COX-2 in both ECs and VSMCs. Whereas these observations integrate hypertension with the mechanism predisposing to thrombosis, overview analysis of controlled clinical trials of NSAIDs detects a stronger predisposition to myocardial infarction than to stroke (22), suggesting that thrombosis is the predominant cause of the excess of cardiovascular events in patients taking COX-2 inhibitors (23).

Finally, it has been suggested that continued elaboration of NO would mask a functional consequence of inhibiting COX-2–dependent PGI_2 formation. Previously, we have shown that deletion of the PGI_2 receptor resulted in thromboxane A_2–dependent cardiovascular phenotypes that were not compensated for by other cardioprotective mechanisms in vivo (8). Here, we show that consequent to deletion of COX-2, globally or selectively in vascular cells, expression of eNOS, release of NO, and NO-dependent vascular relaxation are all depressed. Furthermore, a PGI_2 analog can rescue both the defect in eNOS expression in vitro and the hypertensive phenotype in vivo in the mutant mice.

In summary, placebo-controlled trials have established that NSAIDs selective for inhibition of COX-2 confer a cardiovascular hazard in perhaps 1 to 2% of people exposed, a magnitude of risk similar to that attributable to diabetes or cigarette smoking. Observational studies suggest that this risk may extend to older NSAIDs, such as diclofenac, which similarly exhibit functional selectivity for inhibition of COX-2 (18). Whereas other lines of evidence have emerged consistent with the mechanism that we first proposed on the basis of human genetics, animal models, and randomized trials among NSAIDs, there remained outstanding concerns that we have attempted to address in the current study. Suppression of cardioprotective prostaglandins, particularly PGI_2, in both the vasculature and the cardiomyocytes (24) is sufficient to enhance the risk of thrombosis, hypertension, and heart failure in patients taking NSAIDs. Secondary mechanisms, including suppression of eNOS-dependent elaboration of NO, are likely to contribute to this phenomenon (18).

MATERIALS AND METHODS

Animals

In all cases, transgenic mice deficient in the indicated gene were compared with appropriate strain-, age-, and sex-matched control animals. All mice used in the experiments were on a mixed C57BL/6 × Sv129 genetic background (50%:50%), except the iCOX-2 knockout mice and their $COX\text{-}2^{F/F}$ that were fully backcrossed on C57BL/6. The investigator assessing phenotype was unaware of the genotype throughout these experiments. All animals in this study were housed following guidelines of the Institutional Animal Care and Use Committee (IACUC) of the University of Pennsylvania. All experimental protocols were IACUC-approved.

Generation of vascular COX-2 knockout mice

Mice with the COX-2 gene flanked with two LoxP sites, $COX\text{-}2^{F/F}$ mice, were generated as previously described (24) and crossed with C57BL/6 SM22-Cre mice (25) to obtain VSMC$COX\text{-}2^{-/-}$ mice and with C57BL/6 Tie2-Cre mice (26)to obtain EC $COX\text{-}2^{-/-}$ mice. EC/VSMC double-knockout mice were generated by crossing VSMC $COX\text{-}2^{-/-}$ with EC $COX\text{-}2^{-/-}$ mice. All mutants for experiments were double tail–genotyped to test COX-2 flox recombination (24) and to exclude suspicious Cre germline leakage. SM22 promoter activity

has previously been reported in the developing heart (27). However, genomic analysis of the heart of SM22Cre/flox mice revealed no evidence of Cre-mediated recombination of COX-2^{flox} gene. Gross morphological abnormalities reflective of Tie2 expression in hematopoietic cells were not observed in Tie2Cre/flox mice (28).

Blood pressure measurements

Continuous 24-hour systolic, diastolic, pulse pressure, heart rate, and activity were monitored in the unrestricted animals with the Dataquest IV system (Data Sciences) as described previously (13). Briefly, male and female mice (3 to 4 months old) were anesthetized with ketamine [100 mg/kg, intraperitoneally (ip)] and xylazine (5 mg/kg, ip) and were subjected to surgery under strict sterile conditions. A horizontal incision (right blade to mid-scapular) was made on the back, and the telemetry probe (TA11-PA20; Transoma Medical Inc., Data Sciences International) was inserted. The tip of the transmitter catheter was inserted into the common carotid lumen and advanced until the catheter notch reached the level of the carotid bifurcation. The transmitter signal was monitored with an AM radio tuned to the low end of the dial to verify the proper catheter placement. After surgery, mice were maintained on normal salt intake (0.6% NaCl; diet no. 8746; Harlan Teklad) for a 1-week period, after which the telemetry probes were turned on. The cage with the animal was placed on a receiver plate, and the signal was collected with the Dataquest LabPRO acquisition system (version IV; Transoma Medical Inc., Data Sciences International). Mice were maintained on a 12-hour light/dark regimen and in a sound-attenuated room. Ten-second waveforms of mean arterial pressure, diastolic arterial pressure, systolic arterial pressure, heart rate, and locomotor activity were sampled every 5 min during the 4-day monitoring periods, hourly averages and SD were calculated, and then all the data were expressed as values averaged from daytime (resting phase) and nighttime (active phase) measurements. After this baseline data collection, the probes were then turned off, and the mice were fed a high-salt diet (8% NaCl; diet no. 5008; Harlan Teklad) for 2 weeks (vascular mutants) or 3 weeks (iCOX-2 knockout mice), after which the probes were turned on and the data were collected for 4 days. After the blood pressure on a high-salt diet was recorded, iCOX-2 knockout mice and their controls were injected with cicaprost (1 μg/kg, ip), and blood pressure data were recorded by telemetry for an additional 24 hours. Blood pressure data were calculated 45 min after cicaprost injection.

Intravital microscopy

Mice are anesthetized with an intraperitoneal injection of ketamine (125 mg/kg) and xylazine (12.5 mg/kg) and kept at 37°C using a thermal pad. The scrotum is cut and the cremaster muscle is exteriorized, pinned over the microscopy stage, and bathed in a 37°C bicarbonate-buffered saline aerated with 95% N_2 and 5% CO_2. Digital images of thrombus formation are obtained with an Olympus BX61WI microscope. Wide-field fluorescence microscopy is attained with a 2-Galvo high-speed wavelength changer equipped with a high-intensity 300-W xenon light source. Different excitation filters (360, 480, 575, and 655 nm) are used in this system. The light tube is introduced into the epi-illumination port of the fluorescence microscope. For wide-field imaging, light is amplified up to 1000-fold with a Hamamatsu image intensifier. A Hamamatsu C9300-201 charge-coupled device (CCD) camera captures high-resolution (1390 × 1024) images; it has the highest readout speed available for a digital camera (20 MHz) and allows unbinned full images to be captured at about 20 images per second in a single channel. This Hamamatsu high-speed camera (640 × 480) allows us, with subarrays, to capture up to 60 frames per second, thus enabling us to obtain 20 frames per second for fluorochrome channels. Both high-speed digital cameras are computer-controlled and are cooled to limit dark noise. A Uniblitz shutter on the transmission light source is computer-controlled and can be opened and closed in 50 ms.

This allows us to collect brightfield images while fluorescence images are also being collected.

Laser-induced injury

Arteriolar injury in the cremaster muscle is induced with a fluorescence resonance energy transfer/fluorescence recovery after photobleaching (FRET/FRAP) photoablation system in which the laser tunes to 440 nm, focuses through the microscope objective, parfocal with the focal plane, and aims at the vessel wall. The nitrogen dye laser pulses three to five times at 55 to 65% power, depending on the thickness of the cremaster preparation and the size of the vessel. Successive thrombi will be generated either upstream of the previous thrombus or in different arterioles within the same cremaster preparation.

Image analysis

Image analysis is performed with SlideBook 4.2 software and Dell workstations hardware. A Dell workstation is used to control the components of the imaging system and to collect images. This workstation has two quad-core Xeon 2.66 GHz processors, 4 GB of RAM, two STAT hard drives (1 TB), and a high-end video card. SlideBook, an imaging software package from Intelligent Imaging Innovations, is used for data capture and control for all of the systems: computer, CCD cameras, excitation shutters, Sutter high-speed filter wheels or wavelength changer, Uniblitz shutter, and piezoelectric driver. Data analysis is also performed with SlideBook, using a series of modules that allow image reconstruction, deconvolution, statistics, and volume analysis. To quantify the thrombosis, we calculated the mean background intensity in each image as the average pixel intensity in a defined region of the blood vessel just upstream of the injury and developing thrombus. Circulating fluorescent antibody is the major contributor to the mean background fluorescence. The area of the thrombus is defined as the total number of pixels with fluorescence greater than the average maximal upstream fluorescence during the course of the image capture. To correct for background fluorescence, the mean upstream fluorescence intensity multiplied by the area of the thrombus will be subtracted from the total fluorescence intensity of the thrombus at each time point. The volume of the thrombus will be defined as the number of voxels in all planes at a given time point with fluorescence greater than the maximal background fluorescence.

Isometric tension measurement

Thoracic aortas were cut into rings and mounted in a myograph as described previously (29). Briefly, resting tension was set to 5 mN. After equilibration (at least 60 min at 37°C), rings were precontracted with 3×10^{-7} M phenylephrine, which corresponded to 50% maximum phenylephrine stimulation in gCOX-2 knockout, EC/VSMC double-knockout, and COX-$2^{F/F}$ control mice, and relaxed with 1 μM acetylcholine or 1 μM SNP at 37°C in bubbled (95% O_2/5% CO_2) Krebs-Henseleit (KH) buffer. At the beginning of the experiment, potassium chloride (100 mM) was used to induce maximal contraction. Each experiment was performed in parallel with four aortic rings derived from all mutants.

NO release from mouse aorta

NO release from the endothelial surface of aortas was measured in vitro with a NO-selective microelectrode coupled with an Apollo 4000 Free Radical Analyzer (WPI) as described previously with some modifications (29). Thoracic aortas of gCOX-2 knockout, EC/VSMC double-knockout, and COX-$2^{F/F}$ control mice were carefully isolated and pinned down in KH buffer after connective tissue was thoroughly removed. NO was measured under baseline conditions and after acetylcholine stimulation (10^{-5} M) in the presence or absence

of 1 mM L-NAME. Two measurements were recorded per animal and condition, and NO values were normalized to the weight of the vascular tissue.

Statistics

Statistical analyses were performed with a two-tailed Student's *t* test unless otherwise noted. All values were expressed as means ± SEM. A value of $P < 0.05$ was considered significant. The *P* values for Fig. 3 were obtained by nonparametric two-sample permutation *t* tests. Three types of *P* values were computed: time to max aggregation, max aggregation size, and disaggregation as measured by the AUC over the second half of the measured time span. There were at least two mice in each group and at least 10 measurements per animal.

Supplementary Material

Refer to Web version on PubMed Central for supplementary material.

Acknowledgments

We thank Y. Xiong, J. Zhen, W. Yan, and F. Keeney for excellent technical assistance.

Funding: This study was supported by grants from the NIH (HL-083799 and HL-62250) to G.A.F., the Ministry of Science and Technology of China and National Natural Science Foundation of China (2011CB503906 and 81030004) to Y.Y., the National Institute of Diabetes and Digestive and Kidney Diseases (DK064344) to R.S., and Canadian Institutes of Health Research (MOP-79459 and MOP-93689) to C.D.F. G.A.F. is the McNeill Professor in Translational Medicine and Therapeutics. C.D.F. is the holder of a Tier 1 Canada Research Chair in Molecular, Cellular and Physiological Medicine and is the Career Investigator of the Heart and Stroke Foundation of Ontario.

REFERENCES AND NOTES

1. McAdam BF, Catella-Lawson F, Mardini IA, Kapoor S, Lawson JA, FitzGerald GA. Systemic biosynthesis of prostacyclin by cyclooxygenase (COX)-2: The human pharmacology of a selective inhibitor of COX-2. Proc. Natl. Acad. Sci. U.S.A. 1999; 96:272–277. [PubMed: 9874808]
2. Catella-Lawson F, McAdam B, Morrison BW, Kapoor S, Kujubu D, Antes L, Lasseter KC, Quan H, Gertz BJ, FitzGerald GA. Effects of specific inhibition of cyclooxygenase-2 on sodium balance, hemodynamics, and vasoactive eicosanoids. J. Pharmacol. Exp. Ther. 1999; 289:735–741. [PubMed: 10215647]
3. Moncada S, Vane JR. Prostacyclin and the vascular endothelium. Bull. Eur. Physiopathol. Respir. 1981; 17:687–701. [PubMed: 7034824]
4. Topper JN, Cai J, Falb D, Gimbrone MA Jr. Identification of vascular endothelial genes differentially responsive to fluid mechanical stimuli: Cyclooxygenase-2, manganese superoxide dismutase, and endothelial cell nitric oxide synthase are selectively up-regulated by steady laminar shear stress. Proc. Natl. Acad. Sci. U.S.A. 1996; 93:10417. [PubMed: 8816815]
5. Flavahan NA. Balancing prostanoid activity in the human vascular system. Trends Pharmacol. Sci. 2007; 28:106–110. [PubMed: 17276520]
6. Mitchell JA, Lucas R, Vojnovic I, Hasan K, Pepper JR, Warner TD. Stronger inhibition by nonsteroid anti-inflammatory drugs of cyclooxygenase-1 in endothelial cells than platelets offers an explanation for increased risk of thrombotic events. FASEB J. 2006; 20:2468–2475. [PubMed: 17142796]
7. Grosser T, Yu Y, FitzGerald GA. Emotion recollected in tranquility: Lessons learned from the COX-2 saga. Annu. Rev. Med. 2010; 61:17–33. [PubMed: 20059330]
8. Cheng Y, Austin SC, Rocca B, Koller BH, Coffman TM, Grosser T, Lawson JA, FitzGerald GA. Role of prostacyclin in the cardiovascular response to thromboxane A_2. Science. 2002; 296:539–541. [PubMed: 11964481]
9. Elliott WJ. Do the blood pressure effects of nonsteroidal antiinflammatory drugs influence cardiovascular morbidity and mortality? Curr. Hypertens. Rep. 2010; 12:258–266. [PubMed: 20524091]

10. McGettigan P, Henry D. Cardiovascular risk with non-steroidal anti-inflammatory drugs: Systematic review of population-based controlled observational studies. PLoS Med. 2011; 8:e1001098. [PubMed: 21980265]
11. Krötz F, Struthmann L. A review on the risk of myocardial infarction associated with the NSAID diclofenac. Cardiovasc. Hematol. Disord. Drug Targets. 2010; 10:53–65.
12. Warner TD, Mitchell JA. COX-2 selectivity alone does not define the cardiovascular risks associated with non-steroidal anti-inflammatory drugs. Lancet. 2008; 371:270–273. [PubMed: 18207021]
13. Cheng Y, Wang M, Yu Y, Lawson J, Funk CD, FitzGerald GA. Cyclooxygenases, microsomal prostaglandin E synthase-1, and cardiovascular function. J. Clin. Invest. 2006; 116:1391–1399. [PubMed: 16614756]
14. Yu Z, Crichton I, Tang SY, Hui Y, Ricciotti E, Levin MD, Lawson JA, Pure E, FitzGerald GA. Disruption of the 5-lipoxygenase pathway attenuates atherogenesis consequent to COX-2 deletion in mice. Proc. Natl. Acad. Sci. U.S.A. 2012 10.1073/pnas.1115313109.
15. Yu Y, Stubbe J, Ibrahim S, Song WL, Smyth EM, Funk CD, FitzGerald GA. Cyclooxygenase-2-dependent prostacyclin formation and blood pressure homeostasis: Targeted exchange of cyclooxygenase isoforms in mice. Circ. Res. 2010; 106:337–345. [PubMed: 19940265]
16. Reilly IA, FitzGerald GA. Inhibition of thromboxane formation in vivo and ex vivo: Implications for therapy with platelet inhibitory drugs. Blood. 1987; 69:180–186. [PubMed: 3790723]
17. Hla T, Neilson K. Human cyclooxygenase-2 cDNA. Proc. Natl. Acad. Sci. U.S.A. 1992; 89:7384–7388. [PubMed: 1380156]
18. Grosser T, Fries S, FitzGerald GA. Biological basis for the cardiovascular consequences of COX-2 inhibition: Therapeutic challenges and opportunities. J. Clin. Invest. 2006; 116:4–15. [PubMed: 16395396]
19. Moncada S, Higgs EA, Vane JR. Human arterial and venous tissues generate prostacyclin (prostaglandin X), a potent inhibitor of platelet aggregation. Lancet. 1977; 1:18–20. [PubMed: 63657]
20. Qi Z, Hao CM, Langenbach RI, Breyer RM, Redha R, Morrow JD, Breyer MD. Opposite effects of cyclooxygenase-1 and -2 activity on the pressor response to angiotensin II. J. Clin. Invest. 2002; 110:61–69. [PubMed: 12093889]
21. Kennedy CR, Zhang Y, Brandon S, Guan Y, Coffee K, Funk CD, Magnuson MA, Oates JA, Breyer MD, Breyer RM. Salt-sensitive hypertension and reduced fertility in mice lacking the prostaglandin EP2 receptor. Nat. Med. 1999; 5:217–220. [PubMed: 9930871]
22. Kearney PM, Baigent C, Godwin J, Halls H, Emberson JR, Patrono C. Do selective cyclo-oxygenase-2 inhibitors and traditional non-steroidal anti-inflammatory drugs increase the risk of atherothrombosis? Meta-analysis of randomised trials. BMJ. 2006; 332:1302–1308. [PubMed: 16740558]
23. FitzGerald GA. COX-2 in play at the AHA and the FDA. Trends Pharmacol. Sci. 2007; 28:303–307. [PubMed: 17573128]
24. Wang D, Patel VV, Ricciotti E, Zhou R, Levin MD, Gao E, Yu Z, Ferrari VA, Lu MM, Xu J, Zhang H, Hui Y, Cheng Y, Petrenko N, Yu Y, FitzGerald GA. Cardiomyocyte cyclooxygenase-2 influences cardiac rhythm and function. Proc. Natl. Acad. Sci. U.S.A. 2009; 106:7548–7552. [PubMed: 19376970]
25. Lepore JJ, Cheng L, Min Lu M, Mericko PA, Morrisey EE, Parmacek MS. High-efficiency somatic mutagenesis in smooth muscle cells and cardiac myocytes in SM22α-Cre transgenic mice. Genesis. 2005; 41:179–184. [PubMed: 15789423]
26. Kisanuki YY, Hammer RE, Miyazaki J, Williams SC, Richardson JA, Yanagisawa M. Tie2-Cre transgenic mice: A new model for endothelial cell-lineage analysis in vivo. Dev. Biol. 2001; 230:230–242. [PubMed: 11161575]
27. Miano JM, Ramanan N, Georger MA, de Mesy Bentley KL, Emerson RL, Balza RO Jr. Xiao Q, Weiler H, Ginty DD, Misra RP. Restricted inactivation of serum response factor to the cardiovascular system. Proc. Natl. Acad. Sci. U.S.A. 2004; 101:17132–17137. [PubMed: 15569937]

28. Takakura N, Huang XL, Naruse T, Hamaguchi I, Dumont DJ, Yancopoulos GD, Suda T. Critical role of the TIE2 endothelial cell receptor in the development of definitive hematopoiesis. Immunity. 1998; 9:677–686. [PubMed: 9846489]

29. Pleger ST, Harris DM, Shan C, Vinge LE, Chuprun JK, Berzins B, Pleger W, Druckman C, Volkers M, Heierhorst J, Øie E, Remppis A, Katus HA, Scalia R, Eckhart AD, Koch WJ, Most P. Endothelial S100A1 modulates vascular function via nitric oxide. Circ. Res. 2008; 102:786–794. [PubMed: 18292599]

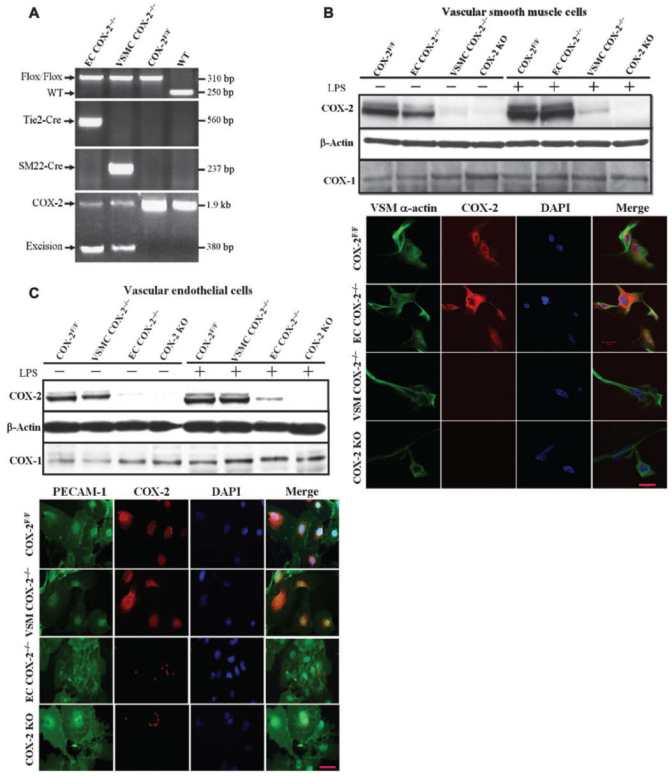

Fig. 1.

Vascular-specific deletion of COX-2. (**A**) Genotyping of vascular COX-2 mutant mice by PCR of genomic DNA extracted from tail biopsies. WT, wild-type. (**B**) COX-1 and COX-2 expression in unstimulated and LPS-stimulated cultured VSMCs. COX-2 protein was barely detectable by Western blot in unstimulated and LPS-stimulated VSMCs from EC COX-$2^{-/-}$, VSMC COX-$2^{-/-}$, and gCOX-2 knockout (KO) mice (top panel). COX-2 protein was not detected by immunostaining in the LPS-stimulated VSMC from VSMC COX-$2^{-/-}$ mice. Primary VSMCs from COX-$2^{F/F}$ control mice, EC COX-$2^{-/-}$ mice, VSMC COX-$2^{-/-}$ mice, and gCOX-2 knockout mice were stained for α-smooth muscle actin (green, ×400) and COX-2 (red, ×400), and nuclei were counterstained with 4′,6-diamidino-2-phenylindole (DAPI) (blue, ×400; lower panel). (**C**) COX-1 and COX-2 expression in unstimulated and LPS-stimulated cultured ECs. COX-2 protein was detected by Western blot in unstimulated and LPS-stimulated ECs in control mice and was almost depleted in the cells from EC COX-$2^{-/-}$ and gCOX-2 knockout mice (top panel). COX-2 protein was not detected by immunostaining in the LPS-stimulated EC from EC COX-$2^{-/-}$ mice. Primary ECs from COX-$2^{F/F}$ control, VSMC COX-$2^{-/-}$, EC COX-$2^{-/-}$, and gCOX-2 knockout mice were stained for platelet endothelial cell adhesion molecule-1 (PECAM-1, green, ×400) and COX-2 (red, ×400), and nuclei were counterstained with DAPI (blue, ×400; lower panel).

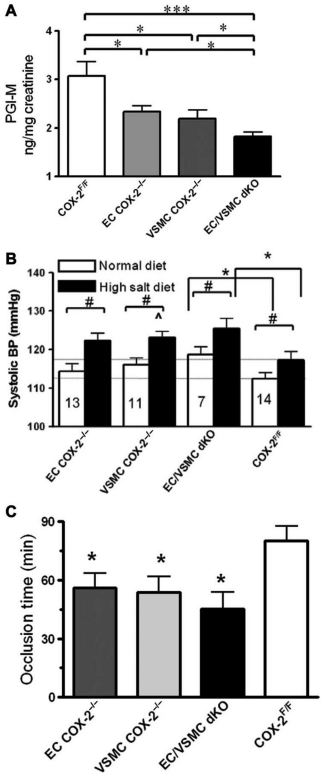

Fig. 2.

Vascular COX-2 deletion depresses PGI-M, elevates blood pressure, and promotes thrombogenesis in mice. (**A**) Twenty-four–hour urine from WT, EC COX-2$^{-/-}$, VSMC COX-2$^{-/-}$, and EC/VSMC COX-2 double-knockout (dKO) mice was collected, and prostanoid metabolites were analyzed by liquid chromatography–mass spectrometry. PGI-M is decreased in EC COX-2$^{-/-}$, VSMC COX-2$^{-/-}$, and EC/VSMC double-knockout mice (8 to 10 weeks old, n = 16 to 22; **P* < 0.05; ****P* < 0.001 versus COX-2$^{F/F}$ control animals). (**B**)Mice (10 weeks old) were implanted with TA11PA-C10 telemetry probes and then, after 1 week's recovery, were placed on a high-salt diet for 2 weeks. Blood pressure (BP) was recorded before (normal diet) and after a high-salt diet. Data are means ± SEM (*n* = 7 to 14). $^{\#}P$ < 0.05 (paired *t* test); **P* < 0.01 (two-tailed unpaired *t* test); ^*P* = 0.05 compared with high-salt-treated COX-2$^{F/F}$ controls. (**C**) The time to thrombotic carotid artery occlusion after photochemical injury was accelerated in EC COX-2$^{-/-}$, VSMCCOX-2$^{-/-}$, and EC/VSMC double-knockout mice (**P* < 0.05 versus COX-2$^{F/F}$ controls).

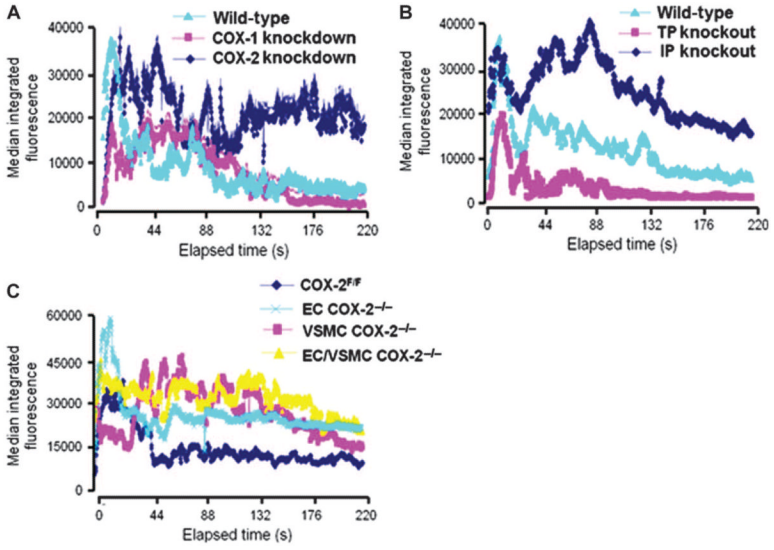

Fig. 3.

Vascular COX-2 restrains thrombogenesis. Shown is thrombogenesis in the cremaster arterioles after laser-induced injury in COX-2 mutant mice, PGI_2 receptor (IP) knockout mice, and thromboxane receptor (TP) knockout mice. Thrombus formation was visualized in real time with fluorescently labeled platelets. (**A** to **C**) Median integrated fluorescence intensity of platelets representing thrombus formation after laser injury for (A) COX-1 knockdown and COX-2 knockdown mice, (B) thromboxane receptor (TP) knockout mice and PGI_2 receptor (IP) knockout mice, and (C) vascular COX-2 knockout mice (20 to 36 thrombi from two to four mice).

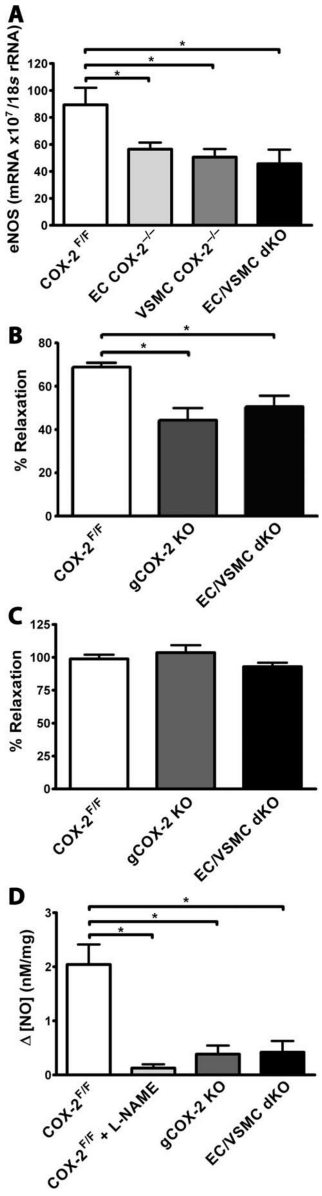

Fig. 4.

COX-2 deletion results in NO-dependent vascular dysfunction. Shown are impaired endothelium-dependent relaxation and NO release in aortas from gCOX-2 knockout and EC/VSMC double-knockout mice. (**A**) eNOS mRNA levels determined by real-time PCR. All samples were normalized to 18*S* rRNA. eNOS mRNA was significantly reduced in aortas from EC COX-$2^{-/-}$, VSMCCOX-$2^{-/-}$, and EC/VSMC double-knockout mice on a high-salt diet for 1 week ($n = 4$ to 6; $^*P < 0.05$). (**B**) Impaired endothelium-dependent vessel relaxation in aortas from gCOX-2 knockout and EC/VSMC double-knockout mice. Acetylcholine-induced relaxation of phenylephrine-preconstricted [median effective concentration (EC_{50})] thoracic aortas was significantly reduced in gCOX-2 knockout mice and in EC/VSMC double-knockout mice compared with COX-$2^{F/F}$ control mice ($n = 3$ to 7; $^*P < 0.05$, one-way ANOVA). (**C**) Direct smooth muscle cell–mediated vessel relaxation of preconstricted aortas using SNP was not different among gCOX-2 knockout, EC/VSMC double knockout, and COX-$2^{F/F}$ control groups. (**D**) NO production measured at the

endothelial surface of thoracic aortas was found to be significantly reduced in COX-$2^{F/F}$ control mouse aortas treated with L-NAME as well as in gCOX-2 knockout and EC/VSMC double-knockout mice (n = 4 to 7; *P < 0.05, one-way ANOVA).